Free Radical Biology and Medicine 65 (2013) 1143–1154

Contents lists available at ScienceDirect

Free Radical Biology and Medicine

journal homepage: www.elsevier.com/locate/freeradbiomed

Original Contribution

The effects of intermittent hypoxia on redox status, NF-κB activation, and plasma lipid levels are dependent on the lowest oxygen saturation

Miguel Quintero [a], María del Carmen Gonzalez-Martin [a], Victoria Vega-Agapito [a], Constancio Gonzalez [a,b], Ana Obeso [a,b], Ramon Farré [b,c], Teresa Agapito [a,b], Sara Yubero [a,b,*]

[a] Institute of Molecular Biology and Genetics, CSIC, Department of Biochemistry and Molecular Biology and Physiology, School of Medicine, University of Valladolid, 47005 Valladolid, Spain
[b] CIBER Enfermedades Respiratorias, Institute of Salud Carlos III, 28029 Madrid, Spain
[c] Unitat de Biofísica i Bioenginyeria, Facultat de Medicina, Universitat de Barcelona–IDIBAPS, Barcelona, Spain

ARTICLE INFO

Article history:
Received 17 March 2013
Received in revised form
1 August 2013
Accepted 23 August 2013
Available online 31 August 2013

Keywords:
Intermittent hypoxia
Oxidative stress
Free radicals

ABSTRACT

Obstructive sleep apnea syndrome (OSAS) is described as repetitive obstructions of the upper airways during sleep, causing concomitant episodes of systemic hypoxia and associated cardiovascular and metabolic pathologies. The mechanisms generating these pathologies are controversial. Because recurrent hypoxia is the element of inadequate respiration that leads to the pathology, experimental models of OSAS consist in the exposure of the animals to intermittent hypoxia (IH) by cycling O_2 percentages in their habitats. A proposed mechanism linking the IH of OSAS to pathologies is the increased production of reactive oxygen species (ROS). However, it has been argued that many patients seem to lack oxidative stress and that, to augment ROS in IH animals, intense hypoxia, seldom encountered in patients, has to be applied. To solve the controversy, we have exposed rats to two intensities of IH (cycles of 10 or 5% O_2, 40 s, and then 21% O_2, 80 s; 8 h/day, 15 days). We then measured reduced and oxidized glutathione and lipid peroxide levels, aconitase and fumarase activities, and ROS-disposal enzyme activity in liver, brain, and lung. Liver levels of nuclear NF-κB-p65 and plasma C-reactive protein (CRP), as well as lipid levels, were also assessed. Lowest hemoglobin saturations were 91.7 ± 0.8 and 73.5 ± 1.4%. IH caused tissue-specific oxidative stress related to hypoxic intensity. Nuclear NF-κB-p65 and lipid content in the liver and CRP in the plasma all increased with IH intensity, as did both plasma triglycerides and cholesterol. We conclude that IH, even of moderate intensity, causes oxidative stress probably related to the pathologies encountered in OSAS patients.

Obstructive sleep apnea (OSA) refers to a repetitive complete or partial obstruction of the upper airways (UAs) occurring every night during sleep time. The cause of OSA is unknown, but mechanical factors narrowing the UAs and some degree of neural brain-stem misregulation of the UA muscle dilators and/or a poor response of these muscles lead to the periodic loss of UA patency during sleep time [1,2]. The number of obstructions/hour defines the apnea–hypopnea index (AHI), the common criterion used to define OSA severity: mild (5–15), moderate (15–30), and severe (>30 obstructions/hour). Because oxygen desaturation is the element in inadequate respiration that most probably leads to systemic pathology [3], the disease severity may be related to nightly oxygen saturation levels: average oxygen saturation ($ASaO_2$), lowest oxygen saturation ($LSaO_2$), percentage of total time with SaO_2 lower than 90% ($T<90\%$), and oxygen desaturation index (ODI; number of desaturations greater than 3%/h). Correlations between AHI and the SaO_2-related indexes have been appreciated differently [4,5].

The arterial decrease in PO_2 and increase in PCO_2 produced in each obstruction activate the carotid body (CB) chemoreceptors, whose increased drive to the brain-stem centers generates an augmented output to the inspiratory and UA dilator muscles and a transient wakening reaction that overcomes the obstruction and restores blood gases [6]. Soon after, another cycle of UA obstruction appears and repeats during sleep. Repetitive awakenings fragment sleep, lessen its restorative nature, and produce diurnal sleepiness, discomfort, and anxiety the following day [7]. Inspiratory efforts with obstructed UAs cause swings in the thoracic pressures and hemodynamic changes that surely contribute to determining the shape of blood and tissue PO_2 oscillations [8,9].

In the long run, OSA generates the obstructive sleep apnea syndrome (OSAS), the combination of OSA and a cohort of associated pathologies, including hypertension and augmented acute vascular accidents, insulin resistance–glucose intolerance, and fatty liver disease, as well as anxiety, depression, and cognitive impairment [10,11,12]. The number and severity of associated comorbidities vary among patients, but sound epidemiologic evidence supports

* Corresponding author at: Institute of Molecular Biology and Genetics, CSIC, Department of Biochemistry and Molecular Biology and Physiology, School of Medicine, University of Valladolid, 47005 Valladolid, Spain. Fax: +34 983 423588.
E-mail address: sarayube@ibgm.uva.es (S. Yubero).

0891-5849/$ - see front matter © 2013 Elsevier Inc. All rights reserved.
http://dx.doi.org/10.1016/j.freeradbiomed.2013.08.180

OSA as a possible factor contributing to these pathologies. Nevertheless, mechanisms linking OSA and associated pathologies remain unsettled. Considering the cardiovascular alterations as paradigmatic pathologies in OSAS, sympathetic hyperactivity and oxidative stress are considered important pathogenic mechanisms [13,14].

Sympathetic hyperactivity and its amelioration with continuous positive airway pressure (CPAP) is a common finding in OSAS patients (e.g., [13,15,16]). Animals exposed to intermittent hypoxia (IH), mimicking the swings in arterial PO_2 and SaO_2 seen in OSAS patients, have allowed sympathetic hyperactivity to be linked with the repetitive CB hypoxic stimulation [17,18]. Oxidative stress would be produced by the repetitive hypoxia–reoxygenation, which, mimicking episodes of ischemia–reperfusion, would generate reactive oxygen species (ROS) and direct vascular endothelium damage [14,19,20]. ROS-regulated transcription factors would cause the overexpression of inflammatory cytokines and vasoconstrictor factors, which damage the endothelium further, thus decreasing vasorelaxant mediators and facilitating atherogenic processes. However, some authors do not find oxidative stress in their OSAS patients [21,22] and, in some studies, the treatment of patients with CPAP did not ameliorate the redox status or the levels of inflammatory markers [23,24]. In animal models, IH causes systemic activation of ROS production, inflammation, and endothelial dysfunction, but the intensities of hypoxia used are higher than those usually encountered in humans (see [13]).

Aiming to clarify these controversies related to the significance of ROS in OSAS, we used two groups of animals exposed to 30 cycles/h, 8 h/day of IH with nadir PO_2 of 5 and 10%. We assessed the redox status with an ample array of biomarkers in liver, lung, and brain tissue and attempted to correlate redox alterations with NF-κB activation, plasma lipid levels, and liver steatosis. We found that IH causes an organ-specific and intensity-related oxidative status. Both levels of IH caused an intensity-related activation of NF-κB in the liver and increased total liver fat and plasma C-reactive protein (CRP), triglycerides, and total cholesterol.

Methods

Animals and anesthesia

Male adult Wistar rats (270–310 g body wt) were housed four per cage, with free access to standard rat solid diet (A04, Panlab SL, Barcelona, Spain) and drinking water. The vivarium maintains controlled conditions of temperature and humidity and a stationary light–dark cycle. The rats were weighed at the start and the end of the experiments (Table 1A). All experimental protocols, except for the IH exposure, were performed in animals anesthetized with sodium pentobarbital (60 mg/kg body wt) administered ip. Blood was withdrawn by direct cardiac puncture. The red blood cell count was made in an Advia flow cytometer (Bayer AG, Leverkusen, Germany; Table 1A).

Experiments were performed in the morning (from 8:30 to 11 AM) of the day after the last hypoxic exposure and the rats were eating and drinking ad libitum until they were brought to the laboratory. In handling the animals we followed the European Community Council Directive of 24 November 1986 (86/609/EEC) for the Care and Use of Laboratory Animals. The Institutional Committee of the University of Valladolid for Animal Care and Use approved the protocols. The animals were euthanized by a cardiac overdose of sodium pentobarbital.

Exposure to IH

Blood gas measurements

The rats were housed in special transparent, hermetically sealed, methacrylate chambers (16 L; four rats/chamber), along with food and water. Each chamber has an inlet for gas entry and, in front of the inlet, inside the cage, 3 cm away of the front wall of the chamber, there is an incomplete wall that breaks the gas jet and allows an even and low velocity flow of gas in the rats' room. At the other end, in the back wall of the chamber, there are two outlets for the exit of the gas. In one of them, there is an O_2 meter to continuously monitor the gas flowing out of the chamber. The desired gas flows into the chamber from gas tanks connected in cascade with stainless steel tubing and intercalated manometers to ensure several days supply of the desired gases. The entry of the various gas mixtures into the chamber is controlled by electrovalves controlled by a microprocessor that allows the time and duration of entry of the desired gas to be determined. The electrovalve system is provided with a battery that ensures the functioning of the entire system in case of electrical power failure. With our system, it is possible to achieve any desired pattern of IH. In the present experiments, the pattern of IH produced was 5 or 10% O_2, 40 s, then 20% O_2, 80 s (i.e., 30 episodes/h), 8 h/day (from 8:00 to 16:00), for 15 days.

In independent groups of rats, one femoral artery of sodium pentobarbitone-anesthetized rats was cannulated and the rats were introduced into the IH exposure chambers (one per chamber). The arterial catheter was taken out of the cages through a hole in the cage cover. The setup allowed anesthesia to be supplemented as required and to anaerobically sample blood at

Table 1
Body weight gain, hematological parameters, blood gases, and hemoglobin saturation indexes in control and 15-day IH (10 and 5% O_2) rats.

Parameter	Experimental group			
	Control 21% O_2	IH 10% O_2	Control 21% O_2	IH 5% O_2
(A) Body weight gain and hematological parameters				
Body weight gain at 15 days (g)	20.2 ± 3.35	26.3 ± 3.08	20.2 ± 3.35	9.8 ± 3.9*
Erythrocytes ($\times 10^6$ mm^{-3})	8.7 ± 0.1	8.5 ± 0.2	7.9 ± 0.2	8.2 ± 0.3
Hemoglobin (g/100 cc)	14.7 ± 0.2	15.6 ± 0.3	14.3 ± 0.2	14.6 ± 0.4
Mean corpuscular volume (μm^3)	55.9 ± 0.6	56.5 ± 1.0	57.6 ± 1.0	57.7 ± 0.9
Mean corpuscular hemoglobin content (pg)	16.7 ± 0.2	18.4 ± 0.4	18.0 ± 0.3	17.8 ± 0.3
(B) Blood gases and hemoglobin saturation indexes				
Arterial PO_2	84.5 ± 2.6	61.3 ± 2.5	84.5 ± 2.6	37.2 ± 0.9
Arterial PCO_2	37.6 ± 1.1	35.0 ± 3.0	37.6 ± 1.1	25.3 ± 2.4
$ASaO_2$ (%)	96.5 ± 0.75	94.9 ± 0.25	96.5 ± 0.35	91.5 ± 0.2
$LSaO_2$ (%)	–	91.7 ± 0.8	–	73.5 ± 1.4
$T < 90\%$ (% exposure time)	–	0	–	25
ODI (times/h)	–	30	–	30
AHI equivalent (times/h)	–	30	–	30

IH, intermittent hypoxia. Data are means ± SEM from 8–10 individual values. *$p < 0.05$.

desired times while the rats remained anesthetized and spontaneously breathing. Blood gas tensions were immediately measured (Automatic Blood Gas System, ABL 5).

Measurement of reduced and oxidized glutathione (GSH and GSSG)

Tissues (liver, lung, and brain) were quickly excised from the animals, washed in ice-cold saline, dry-blotted on filter paper, weighed, and placed in Eppendorf tubes containing a solution of 5-sulfosalicylic acid (SSA) at 5% and 0.25 mM EDTA; SSA solution volume was adjusted to 5 × tissue weight. Tissues were stored at −80 °C until assay or immediately glass-to-glass homogenized at 0–4 °C and centrifuged in a microfuge (4 °C, 10 min) and the supernatant was used to measure GSH and GSSG. Reduced and oxidized glutathione was determined by the Griffith method, as recently described in detail [25]. From GSH and GSSG levels, the glutathione redox potential (E_{GSH}) was calculated using the Nernst equation, $E_{GSH} = E^{\circ\prime}_{GSH} - RT/zF \times \ln [GSH]^2/[GSSG]$, and a value for $E^{\circ\prime}_{GSH}$ of −240 mV.

Measurement of lipid peroxides (LPOs)

Tissues (liver, lung, and brain) were homogenized in 20 mM phosphate buffer (pH 7.4; wet tissue wt/buffer volume 0.2) and separated into three aliquots: one aliquot was used to determine LPOs, the second aliquot was used to determine protein levels, and the third was used to determine glutathione peroxidase (GPx) activity. The LPO aliquot was treated with 10 μl/ml 0.5 M butylated hydroxytoluene in acetonitrile to prevent the oxidation of the sample. The LPO levels were determined immediately according to the instructions given by the supplier of the assay kit (Bioxytech LPO-586; Oxis Health Products, Portland, OR, USA). Being aware of the difficulties of selecting a method to measure LPO [see 26], we chose an assay that, fulfilling the requirements of sensitivity and reproducibility, is reasonable in cost and convenient in handling in the context of this study. In the assay, malonaldehyde and 4-hydroxyalkenals react with a chromogen reagent at low temperature yielding a stable chromophore with peak absorbance at 586 nm. This assay has been found to provide a convenient index of lipid peroxidation: the low-temperature formation of the chromophore and the prevention of the oxidation of the tissue homogenate secure the adequate stability of the analytes and the specificity of the assay [27].

Measurement of aconitase and fumarase activities

The activities of both enzymes aconitase and fumarase were determined as described by Couplan et al. [28]. Fresh tissues were minced in ice-cold TES buffer (10 mM Tris, pH 7.4, 250 mM sucrose, and 1 mM EDTA) and mitochondria were isolated as described by Pecqueur et al. [29]. The final mitochondrial pellet was resuspended in the same TES buffer and mitochondria were lysed by the addition of Triton X-100 at a final concentration of 0.5% w/v. Aliquots of 20, 40, and 10 μl of mitochondrial lysates from liver, lung, and brain, respectively, were used for enzymatic measurements. Enzymatic reactions run for 8 min in the appropriate medium: 30 mM sodium isocitrate, 50 mM Tris–HCl, pH 7.4, 0.6 mM $MnCl_2$ for aconitase [30] and 50 mM sodium L-malate, 50 mM sodium phosphate buffer, pH 7.4, for fumarase [31]. The enzymatic activities were assessed following the increase in optical density at 240 nm. The increase in linear rates of optical density over the last 3 min was taken as a measure of enzymatic activity. The aconitase/fumarase ratio was expressed as the ratio of the respective linear rates of optical density increase.

Measurement of GPx activity

GPx activity was assayed as described by Paglia and Valentine [32]. The assay measures the disappearance of NADPH due to a coupled reaction: first, GPx oxidizes GSH to GSSG in the presence of peroxide and second, GSSG is reduced back to GSH by glutathione reductase using NADPH as the donor of reduction equivalents. The activity of GPx in the sample (Δabsorbance min^{-1}) was calculated on the basis of the molar extinction coefficient for NADPH (6220 UA mol^{-1}). One unit of activity is equal to 1 μmol NADPH oxidized min^{-1} mg^{-1} protein.

Catalase activity in tissues

Catalase activity was assayed using a modified version of the method of Aebi [33]. Tissues were homogenized in cold 50 mM phosphate buffer (pH 7; wet tissue wt/buffer volume 0.05 to 0.10) containing 1 mM EDTA and 0.1% Triton X-100. After centrifugation (10,000*g;* 15 min; 4 °C) supernatants were immediately used to measure catalase activity or stored at −80 °C until the assay.

An aliquot of supernatant (10–20 μl) was incubated for 1 min at 25 °C with an excess of H_2O_2 (50 mM) generating water and oxygen. The reaction was stopped by the addition of 900 μl of 15 mM sodium azide and 10 μl was assayed to evaluate the remaining H_2O_2. The remaining H_2O_2 reacts with a color reagent (150 mM potassium phosphate buffer, pH 7, containing 0.25 mM 4-aminoantipyrine, 2 mM 3,5-dichloro-2-hydroxybenzenesulfonic acid, and 0.7 U ml^{-1} peroxidase) and generates a red quinoneimide dye that absorbs at 520 nm. Standard curves were constructed in parallel with concentrations of hydrogen peroxide between 1.25 and 7.5 mM. Samples without tissue homogenate, but with H_2O_2 (50 mM), were used to obtain the maximum rate of formation of red quinoneimide, and the H_2O_2 destroyed by the catalase present in the tissue homogenates and transformed in enzymatic activity was calculated by subtraction. One unit of catalase activity equals 1 μmol of H_2O_2 degraded min^{-1} mg^{-1} protein at pH 7 at 25 °C at a substrate concentration of 50 mM H_2O_2.

Superoxide dismutase (SOD) activity in tissues

The tissues (liver, lung, and brain) were homogenized in cold 0.25 M sucrose buffer (pH 7.4; w/v 0.1) containing 10 mM Tris and 1 mM EDTA. The homogenates were centrifuged and the supernatant was immediately used to measure SOD activity or stored at −80 °C until the assay. The SOD activity was determined using an indirect method (SOD determination kit; Fluka, Madrid, Spain). Potassium cyanide (3 mM), which inhibits cytosolic SOD, was allowed to differentially determine mitochondrial and cytosolic SOD activities. SOD is expressed as activity units, 1 U being the amount of enzyme capable of inhibiting, by 50%, the reduction of the cytochrome *c* in a coupled system with xanthine oxidase at pH 7.8 and 25 °C in a 3-ml reaction mixture.

Western blot analysis

The general procedure of SDS–PAGE and immunoblotting has been previously described [34]. Liver tissue was homogenized in lysis buffer (100 mg tissue/300 μl buffer; lysis buffer composition was sacarose, 250 mM; EDTA, 1 mM; Hepes, 10 mM; pH 7.5) containing a Protease Inhibitor Cocktail and Phosphatase Inhibitor Cocktail (Sigma, Madrid, Spain) at the usual concentration. The supernatant resulting from an initial low-speed centrifugation to discard the nuclear fraction was centrifuged (16,100*g*, 45 min, 4 °C) to obtain a new supernatant corresponding to the cytoplasmic fraction for Cu,Zn-SOD and catalase assay. The pellet was resuspended in lysis buffer (0–4 °C) containing 1% SDS + 1 mM dithiothreitol, and after frequent vortexing for 30 min, the sample was recentrifuged (16,100*g*, 30 min, room temperature) and the supernatant (mitochondrial fraction) saved for Mn-SOD assays. Samples containing 50 μg protein were electrophoretically fractionated on 12% SDS–polyacrylamide gels and protein bands transferred to polyvinylidene difluoride membranes by electroblotting (Mini Trans-Blot cell transfer, Bio-Rad, Hercules, CA, USA). Membranes were blocked (5% nonfat dry milk in Tris-buffered saline (TBS))

and incubated overnight (4 °C in TBS containing 0.1% Tween 20 and 0.5% bovine serum albumin) with primary antibodies: anti-Cu, Zn-SOD (rabbit antiserum; Millipore; 1:5000), anti-Mn-SOD (rabbit antiserum; Millipore; 0.5 μg/ml), anti-catalase (rabbit antiserum; Novus Biologicals; 1:3000), and anti-β-actin (mouse antiserum; Sigma; 1:5000). After being washed, the membranes were reincubated with secondary horseradish peroxidase-conjugated goat anti-rabbit IgG (Millipore, 1:20,000, for catalase and SODs) and goat anti-mouse IgG (BD Pharmingen, 1:1000, for β-actin). Membrane signals were ECL-developed (PerkinElmer) and visualized automatically (Versadoc; Quantity One 4.5.2; Bio-Rad) or conventionally in a manual manner using ECL-sensitive film (Amersham Hyperfilm). For internal normalization, in all the cases, β-actin signals were obtained after stripping and reprobing of the corresponding membranes. Optical densities of the bands were determined with ImageJ software and normalized with corresponding β-actin signals to correct for minor deviations in protein loading. Normalized values were then averaged for all the replicated gels and used to calculate the relative change in enzyme expression in each group of animals.

CRP levels in plasma

A commercial kit for rat CRP was used to assess the levels of this acute-phase marker. Sample handling and CRP measurement were carried out following protocols provided by the supplier (Cusabio Biotech, bioNova Cientifica, Madrid, Spain).

Analysis of NF-κB activity in the liver

To determine active NF-κB-p65 activity in livers, nuclear extracts were prepared using the Nuclear Extract Kit (No. 40010; Active Motif, Rixensart, Belgium) and the nuclear protein content of the samples was determined by the method of Bradford. Samples of nuclear extracts containing equal amounts of protein were used in the NF-κB-p65 TransAM Transcription Factor Assay Kit 40096 (Active Motif). The assays were performed according to the manufacturer's instructions. Activation was detected by incubation with the primary antibody anti-NF-κB, which specifically recognizes an epitope (p65) accessible only when the factor is activated and bound to its DNA target. A secondary anti-IgG horseradish peroxidase conjugate allows detection of the activated NF-κB spectrophotometrically (450 nm). Data are presented as control fold increase.

Total lipid content in liver

Total lipids in liver were obtained following the solvent extraction method of Folch et al. and gravidimetrically assessed [35]. The extracted material was transferred to small petri dishes and dried until two successive weights were identical. Results are expressed as percentage of total weight of the original piece of liver tissue.

Triglyceride and total cholesterol levels in plasma

Plasma triglyceride and total cholesterol levels were spectrophotometrically determined using kits obtained from Chemelex (Labkit; Chemelex SA, Barcelona, Spain).

Statistics

All data are expressed as the mean ± SEM. The significance of the differences between the means was calculated by one-way analysis of variance with Dunnett's multiple comparison tests, respectively. A p value of 0.05 or less was considered to represent a significant difference.

Results

Experimental animals

The animals tolerated well both intensities of hypoxia. There were no losses of animals and their weight gain in 10% O_2 IH was not different from that of the controls, although the animals exposed to 5% O_2 IH gained weight at a lower rate (Table 1A). However, the red blood cell count and related parameters, including hemoglobin, mean corpuscular volume, and mean corpuscular hemoglobin content, did not show significant differences between controls and both groups of IH animals. These findings show evidence that the episodes of IH in rats, as well as in OSAS patients [36,37], do not activate erythropoiesis (Table 1A). Table 1B shows blood gases and hemoglobin saturation parameters in our animals measured over several IH cycles. PO_2 was in the range 80–95 mm Hg when the cages were fluxed with air, in the periods immediately before the hypoxic episodes. The lowest value of PO_2 registered during the 10% O_2 hypoxic episodes was 61.3 ± 2.5 mm Hg ($n=8$), falling to 37.2 ± 0.9 mm Hg ($n=8$) during the 5% O_2 hypoxic episodes. In all likelihood, the real level of hypoxia attained was a little more intense because the nadir of PO_2 in the chamber lasted a few seconds and the withdrawal of blood took 20 s. PO_2 in blood samples withdrawn immediately after the hypoxic episodes recovered to control values. Arterial PCO_2 dropped from prehypoxic levels of 37.6 ± 1.1 to 35 ± 3 and 25 ± 2 mm Hg with the 10 and 5% O_2 IH, respectively. In the immediately posthypoxic period, PCO_2 remained below the control value, to recover before the onset of the next episode of hypoxia. The changes in PCO_2 clearly evidence the hyperventilation triggered by hypoxia. Hemoglobin O_2 percentage before hypoxic episodes was 96.5 ± 0.75%, reaching its lowest mean values of 91.7 ± 0.8 and 73.5 ± 1.4% during the 10 and 5% O_2 episodes. The $ASaO_2$ dropped from 96.5 ± 0.75% in the control prehypoxic exposure period to 94.9 ± 0.25% (10% IH) and to 91.5 ± 0.20% (5% IH), with the lowest saturations, respectively, of 91.7 ± 0.80 and 73.5 ± 1.40%. $T<90\%$ was 0 in 10% O_2 and reached 25% of the duration of the exposure at 5% O_2. As expected, the ODI was, in both cases, 30 times/h, identical to AHI.

Glutathione levels and glutathione redox potentials in brain, liver, and lung

Table 2 shows the levels of GSH and GSSG and the GSH/GSSG ratios encountered in brain, liver, and lung tissues of the control, 10% O_2, and 5% O_2 IH animals. Note that whereas brain and lung tissues have total glutathione levels close to 1.5–2 μmol/g wet tissue, liver has levels nearly five times larger. Note also that GSH/GSSG ratios are higher than 50 in the three tissues, implying that most of the glutathione encountered in the three tissues and under the three experimental conditions is in the GSH form. The calculation of E_{GSH}, which accurately reflects the general redox environment of cells [38], evidences (Fig. 1) that the intensity of our IH protocol did not cause significant permanent diminution of the redox buffer power of the cells.

LPO levels in brain, liver, and lung

Several ROS species (hydroxyl or perhydroxyl radicals) can attack unsaturated fatty acids of the cell membranes to produce their peroxidation and fragmentation with the release of LPO. Therefore the level of LPO represents a marker of the oxidative attack of cell membranes [39]. Fig. 2 shows LPO levels (measured as malonaldehyde + 4-hydroxyalkenals) in the brain, liver, and lung homogenates of control and IH animals of both intensities. Note, first, that levels of LPO in the lung in control animals are nearly double those in the brain and liver. Note second that IH hypoxia increased LPO in

liver tissue, but not in brain or lung. This LPO increase, although moderate, paralleled the intensity of IH and reached a 22% increase with the 5% O_2 IH. In aortas of the 5% O_2 IH animals, LPO levels were also no different from those encountered in control animals (0.57 ± 0.04 vs 0.52 ± 0.05 nmol/mg/protein; $n=10$; $p > 0.05$).

Aconitase/fumarase activities

Mammalian aconitase contains a $[4Fe–4S]^{2+}$ cluster as a prosthetic group, which is susceptible to inactivation by oxidants, particularly $O_2^{\bullet -}$ and hydrogen peroxide. These two, and another ROS, lead to the release of Fe-α from the enzyme $[4Fe–4S]^{2+}$ cluster and the formation of a $[3Fe–4S]^{1+}$ cluster. This process renders the enzyme inactive, incapable of interconverting citrate and isocitrate and making aconitase activity an adequate index of mitochondrial oxidative damage [40]. On the other hand, fumarase, another tricarboxylic acid cycle enzyme, is resistant to oxidative damage [41], making the ratio of aconitase/fumarase activities measured in the same tissue samples a very reliable index of mitochondrial oxidative damage. Fig. 3 shows the ratios of aconitase/fumarase activities in brain, liver, and lung tissues. Note, first, the differences in activity ratios between the three different tissues. Note also that 5% O_2 IH caused very significant decreases in the ratio of aconitase/fumarase activity in the three tissues. The 10% O_2 IH caused only a minor, but statistically significant, decrease in brain.

Table 2
Reduced and oxidized glutathione (GSH, GSSG) levels and GSH/GSSG ratios in brain, liver, and lung homogenates of control and intermittent hypoxia (IH)-exposed rats.

Parameter	Tissue	Experimental group		
		Control	IH 10% O_2	IH 5% O_2
GSH (μmol/g tissue)	Brain	1.6 ± 0.04	1.7 ± 0.04	1.6 ± 0.03
GSH (μmol/g tissue)	Liver	7.8 ± 0.2	7.4 ± 0.9	8.2 ± 0.3
GSH (μmol/g tissue)	Lung	2.0 ± 0.04	2.0 ± 0.05	2.2 ± 0.06
GSSG (μmol/g tissue)	Brain	0.006 ± 0.001	0.008 ± 0.001	0.006 ± 0.001
GSSG (μmol/g tissue)	Liver	0.1 ± 0.01	0.1 ± 0.01	0.1 ± 0.01
GSSG (μmol/g tissue)	Lung	0.04 ± 0.003	0.04 ± 0.002	0.04 ± 0.004
[GSH]/[GSSG]	Brain	229 ± 34	208 ± 11	257 ± 20
[GSH]/[GSSG]	Liver	100 ± 10	94 ± 10	91 ± 9
[GSH]/[GSSG]	Lung	58 ± 5	53 ± 4	64 ± 8

Data are means ± SEM from 20 (control) and 9 or 10 (IH) individual values.

Activities of ROS disposal enzymes

A general response of cells to an oxidative insult is the upregulation of protective antioxidant gene expression, particularly of ROS-disposing enzymes [39]. $O_2^{\bullet -}$ and H_2O_2 are the two major primary ROS [25], and the former is rapidly transformed into the latter, either spontaneously (spontaneous dismutation) or enzymatically with the cooperation of superoxide dismutases. Therefore, H_2O_2 represents the common final path of ROS. Along with these general concepts we have measured the activities of Mn-SOD (mitochondrial) and Cu,Zn-SOD (cytoplasmic), GPx, and catalase in brain, liver, and lung. The last two enzymes are those mainly responsible for H_2O_2 disposal in cells.

Superoxide dismutases

Fig. 4 shows the activities of Mn-SOD and Cu,Zn-SOD in brain, liver, and lung homogenates and the level of expression of both enzymes in liver. Note first that, as is the case in human tissues [42], most of the dismutating activity is in the form of the cytosolic Cu,Zn-enzyme (see also [43]). Note second that SOD activity is about five times higher in the liver than the in brain and lung, which have comparable activity levels (see [42]). Note finally that, in contrast to the expected upregulation of SOD, what we found was a decrease in both enzyme isoforms in the liver with both intensities of IH; in the lung, both isoforms of SOD decreased, but only with the lower IH intensity, and in brain only the activity of the mitochondrial isoform

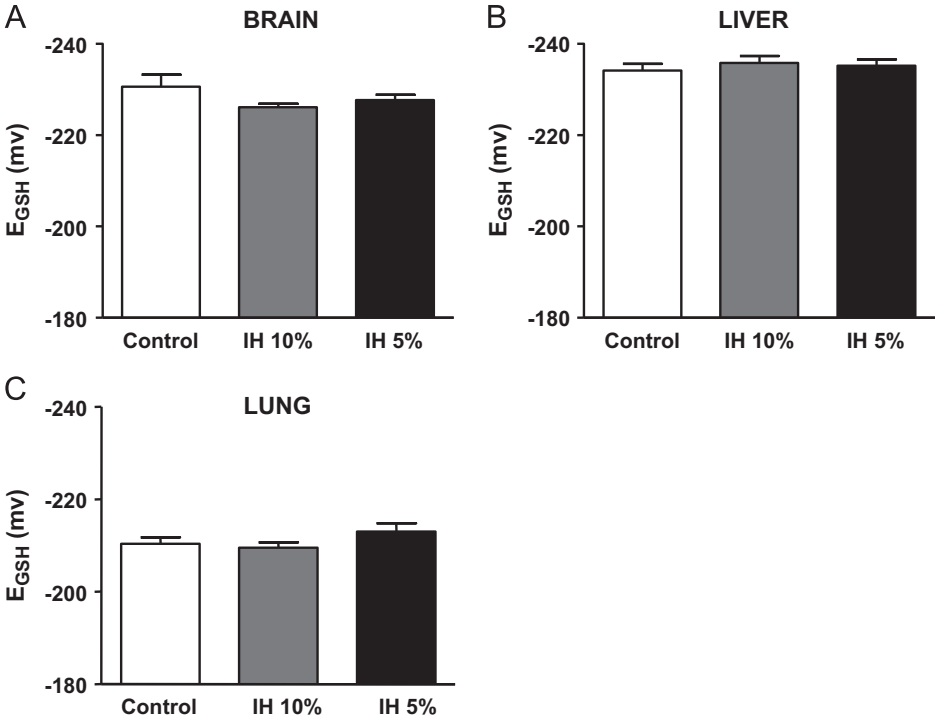

Fig. 1. Glutathione redox potentials, E_{GSH}, in (A) brain, (B) liver, and (C) lung of control and 10 and 5% O_2 intermittent hypoxic rats. Note that brain and liver exhibit slightly more negative E_{GSH} than lung in control animals and that IH did not cause significant variations in the potential in any tissue. Data are means ± SEM from 20 (control) and 9 or 10 (IH) individual values.

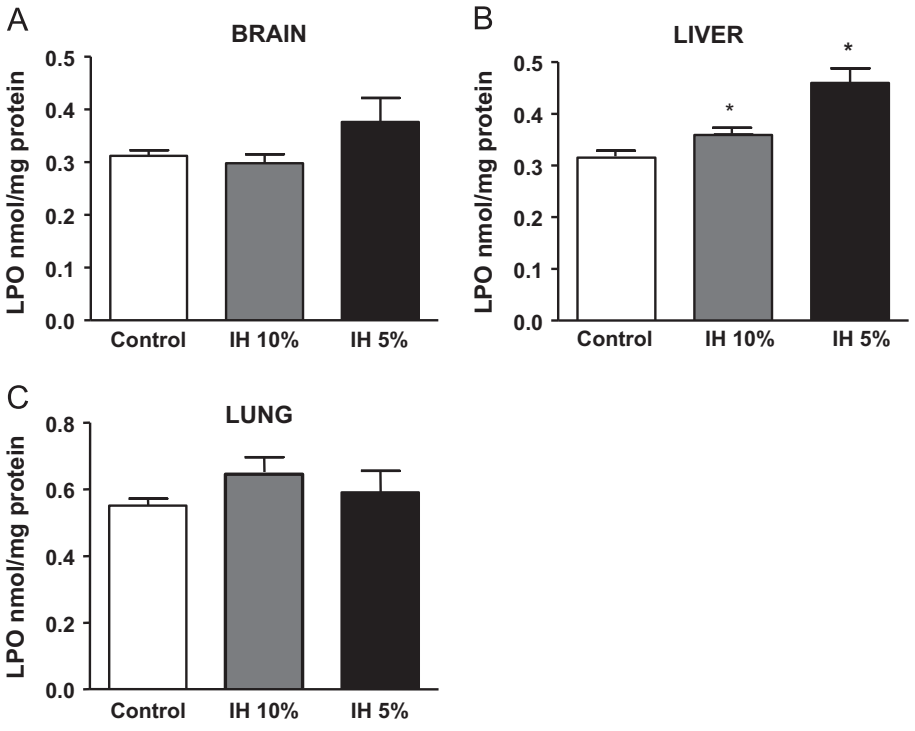

Fig. 2. Lipid peroxide levels in (A) brain, (B) liver, and (C) lung of control and 10 and 5% O_2 intermittent hypoxic rats. LPO correspond to malonaldehyde + 4-hydroxyalkenals. Data are means ± SEM from 20 (control) and 9 or 10 (IH) individual values. *$p < 0.05$ vs corresponding control.

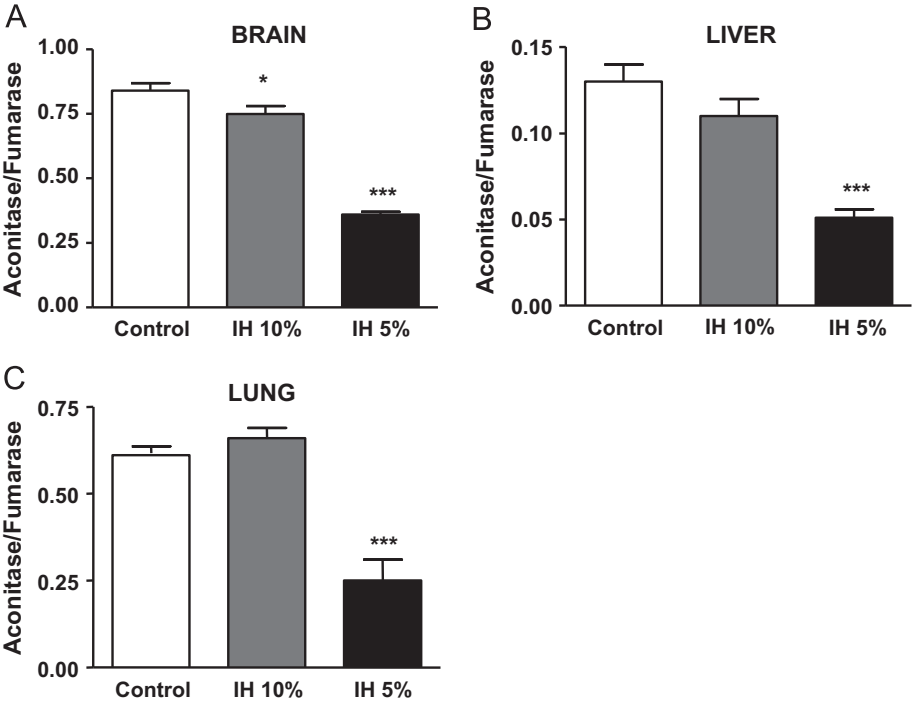

Fig. 3. Ratios of aconitase/fumarase activities, in (A) brain, (B) liver, and (C) lung of control and 10 and 5% O_2 intermittent hypoxic rats. Note the variable ratio of activity in the three tissues in control animals and its decrease in the three tissues in proportion to the intensity of the IH. Data are means ± SEM from 20 (control) and 9 or 10 (IH) individual values. *$p < 0.05$ and ***$p < 0.001$ vs corresponding control.

decreased for 5% IH. These unexpected findings indicate that the control of SOD activity is more complex than a simple substrate regulation as suggested in the preceding paragraph. In fact, as Fig. 4D shows, the expression of Cu,Zn-SOD in liver was not significantly affected by either level of IH, whereas the level of expression of Mn-SOD was significantly diminished by both intensities of IH. Note, however, that diminution of the Mn-SOD protein is smaller than the decrease in the level of activity, indicating that IH lowers the specific activity of the expressed enzyme; this diminution of the specific activity is also evident for the cytoplasmic enzyme.

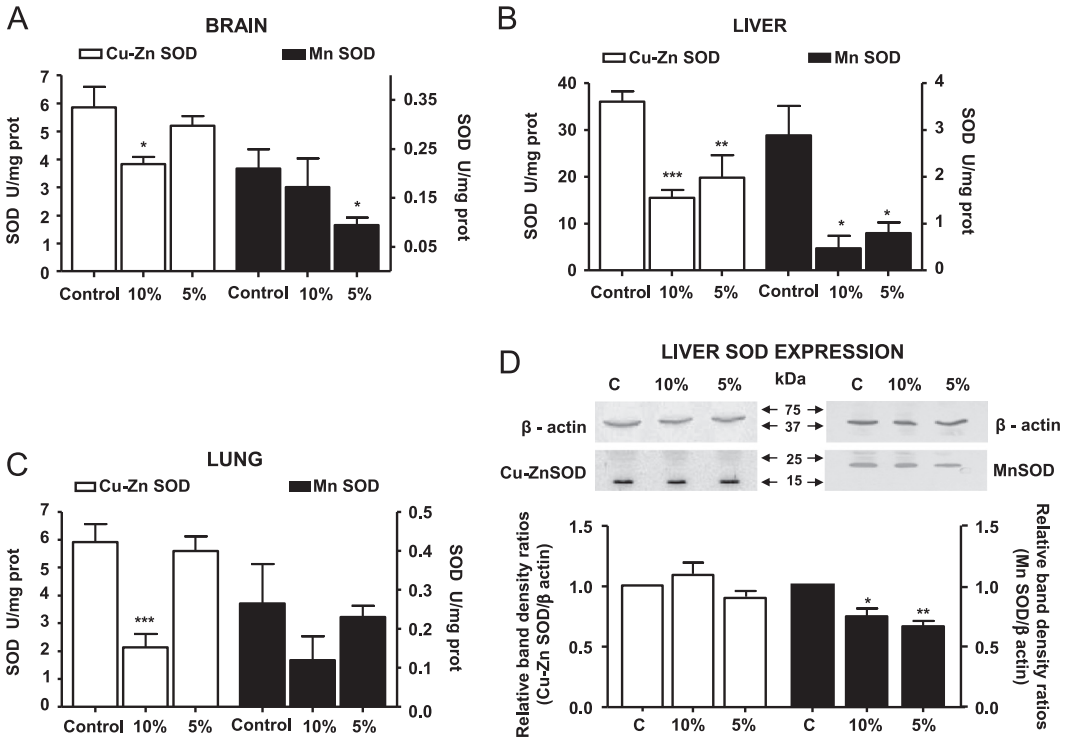

Fig. 4. Activities of superoxide dismutases, Mn-SOD (mitochondrial) and Cu,Zn-SOD (cytosolic), in (A) brain, (B) liver, and (C) lung homogenates of control and 10 and 5% O_2 intermittent hypoxia rats. Data are means ± SEM from 20 (control) and 9 or 10 (IH) individual values. *$p < 0.05$, **$p < 0.01$, and ***$p < 0.001$ vs corresponding control. (D) The level of expression of both enzymes in liver of control and 10 and 5% O_2 IH animals expressed as the ratio of the density of the SOD to the β-actin bands. In every immunoblot the SOD/β-actin ratio in the liver samples of control animals was taken as a unit. The bands presented here were isolated from full immunoblots (supplementary material). Data are means ± SEM of seven individual values (*$p < 0.05$; **$p < 0.01$).

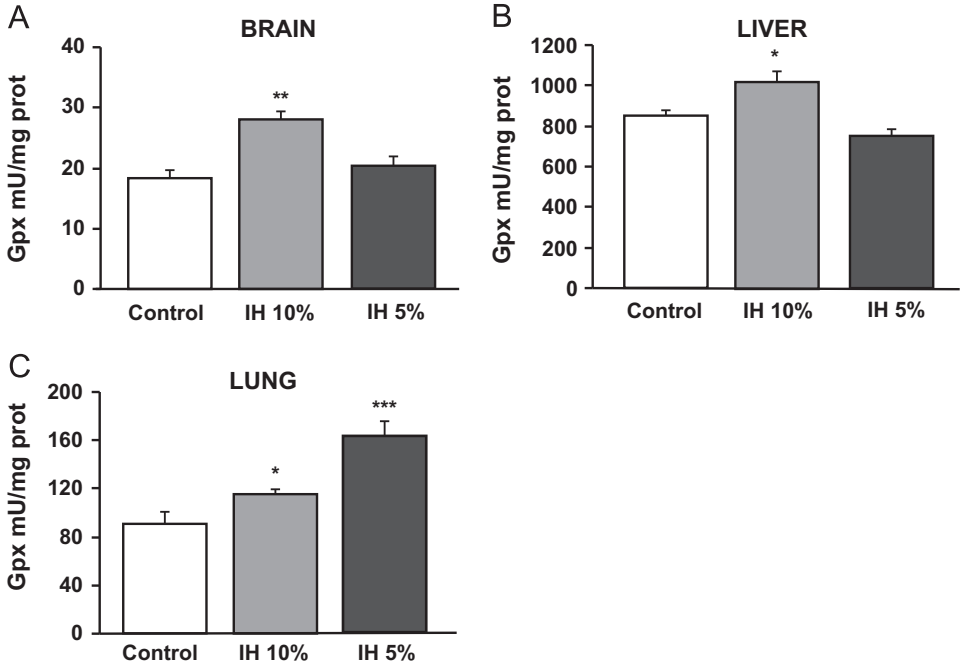

Fig. 5. Glutathione peroxidase activities in (A) brain, (B) liver, and (C) lung homogenates of control and 10 and 5% O_2 intermittent hypoxia rats. Data are means ± SEM from 20 (control) and 9 or 10 (IH) individual values. *$p < 0.05$, **$p < 0.01$, and ***$p < 0.001$ vs corresponding control.

Glutathione peroxidase

The main function of GPx is to reduce the H_2O_2 resulting from the action of SOD on water. The activities of GPx in the brain, liver, and lung of control and 5 and 10% IH hypoxic animals are shown in Fig. 5. The three tissues exhibited significantly augmented activities of GPx with the lower intensity of IH. The more intense IH markedly augmented the activity of GPx, but exclusively in the lung.

Catalase

As with the previous enzymes, the activity of catalase in the liver highly exceeded that encountered in lung (about 20 ×) and brain tissue (about 100 ×). IH did not modify catalase activity in either brain or lung, but in the more intense IH caused a significant decrease in the liver (Figs. 6A–C). Fig. 6D shows the levels of expression of catalase in liver tissue of control and 10 and 5% O_2

IH. Data indicate that the most intense IH caused a decrease in catalase expression in a magnitude comparable to the decrease in activity, implying that the expressed enzyme exhibits normal activity.

NF-κB activation in the liver

NF-κB is a transcription factor known to have an ample array of cellular functions, including the regulation of the expression of inflammatory cytokines. ROS have been shown to represent common, but not universal, second messengers for NF-κB activation, i.e., ROS activation of NF-κB is to some extent cell-type specific [44]. We therefore we wanted to study whether the liver, the studied tissue with the most marked oxidative stress and the key player in the metabolic disorders present in OSAS patients, exhibits higher than normal levels of NF-κB activation. Fig. 7A shows that, indeed, IH augmented, in an intensity-dependent and statistically significant manner, the level of activation of NF-κB.

C-reactive protein (CRP) levels in plasma

CRP is an acute-phase reactant primarily synthesized in hepatocytes in response to inflammation mediators and released to plasma; in turn, CRP binding to cells may trigger the generation of ROS, creating a vicious cycle that can lead to the development of chronic inflammation [45]. According to this physiopathological schema, Fig. 7B shows that plasma CRP levels increased with the intensity of IH and, further, in experiments currently in progress we have observed that CRP continues to increase if the duration of IH is prolonged (data not shown).

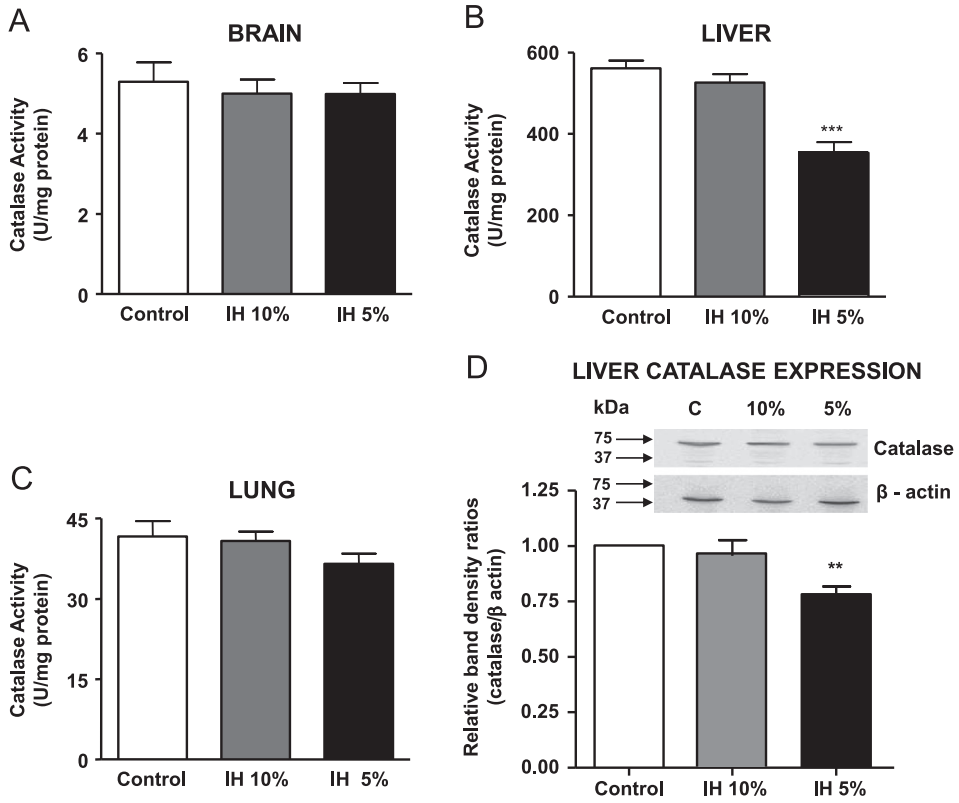

Fig. 6. Catalase activity in (A) brain, (B) liver, and (C) lung homogenates of control and 10 and 5% O_2 intermittent hypoxia rats. Data are means ± SEM from 24 (control) and 13 or 14 (IH) individual values. ***$p < 0.001$ vs corresponding control. (D) The level of expression of catalase in liver of control and 10 and 5% O_2 IH animals expressed as the ratio of density of the catalase to the β-actin bands. The bands presented here were isolated from full immunoblots (supplementary material). In every immunoblot the catalase/β-actin ratio in the liver samples of control animals was taken as unit. Data are means ± SEM of seven individual values (**$p < 0.01$).

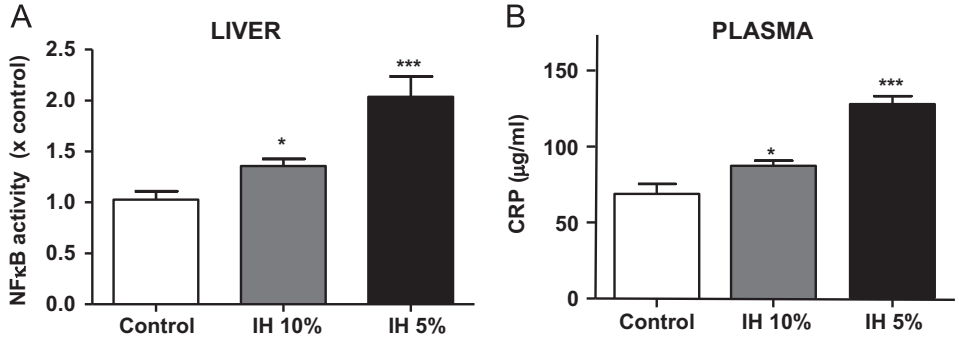

Fig. 7. (A) Nuclear NF-κB-p65 activity in liver and (B) plasma levels of C-reactive protein in control and 5 and 10% IH animals. Data are means ± SEM from 18 (control) and 9 (IH) individual values. *$p < 0.05$; ***$p < 0.001$ vs corresponding control.

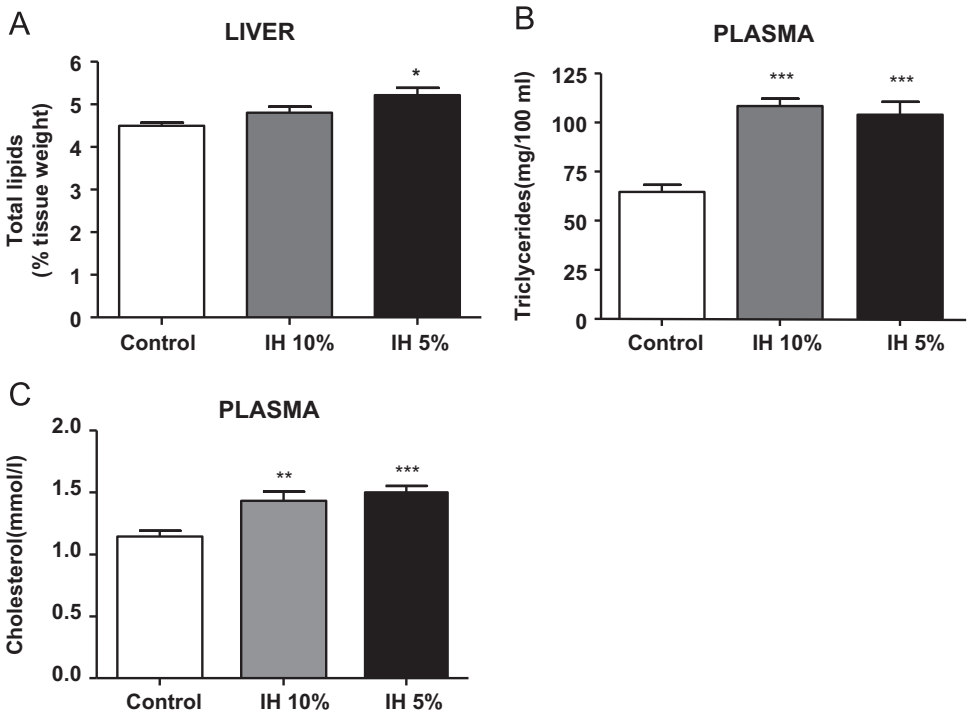

Fig. 8. (A) Liver lipid content (% of total tissue weight) and plasma levels of (B) triglycerides and (C) total cholesterol in control and 5 and 10% IH animals. Data are means ± SEM from 18 (control) and 9 (IH) individual values. *$p < 0.05$; **$p < 0.01$; ***$p < 0.001$ vs corresponding control.

Total lipid content in the liver and plasma triglyceride and cholesterol levels

Nonalcoholic fatty liver disease refers to a wide spectrum of liver disease not linked to alcohol drinking, ranging from steatosis (simple fatty liver) to steatohepatitis and cirrhosis. Although the intimate pathogenesis of NASH is not well understood, it is known that oxidative stress and insulin resistance are major contributors in the pathogenesis and progression of nonalcoholic fatty liver disease [46]. In fact, in in vivo [47] and cell culture models [48] it has been shown that antioxidants prevent lipid accumulation in cells. Consistent with these notions, Fig. 8A shows that total lipid content in the liver was augmented with IH, the increase reaching statistical significance with the more intense hypoxia. Accompanying the steatosis, Figs. 8B and C show that there was a significant increase in plasma triglycerides and total cholesterol levels, this being statistically significant at both intensities of IH.

Discussion

Of the three groups of data provided by our study, those presented in Figs. 1 to 3 (E_{GSH}, LPO levels, and aconitase/fumarase ratios) reflect the actual situation of the redox status in our animals and indicate that IH does indeed produce oxidative stress. The second group of data relate to ROS-disposal enzymes (Figs. 4–6; superoxide dismutases, glutathione peroxidase, and catalase); again the data corroborate the oxidative distress by evidencing the fact that cellular enzymes devoted to maintaining the oxidant–antioxidant equilibrium are altered. However, these alterations of antioxidant enzymes could be a primary effect of IH, and therefore the cause of the oxidative stress, or they could be a consequence of oxidative stress. Finally, the third group of data (Figs. 7 and 8; NF-κB activation, C-reactive protein, and alterations in lipid metabolism) are parameters mechanistically associated with oxidative stress. The discussion that follows is devoted to highlighting the significance of our data in the field of IH and OSAS, the potential mechanisms causing increased ROS production in IH, as well as the mechanisms leading to alterations in the activities of ROS-disposal enzymes and those leading to the activation of NF-κB and lipid alterations. The final paragraphs of the discussion are devoted to presenting the limitations and strengths of our study and the overall conclusions.

The ample array of markers measured in assessing the oxidative stress, along with the double intensities of IH used and the multiple tissues tested, has provided clarifying results evidencing that not all markers detect oxidative stress and that different tissues respond to the IH challenge in specific manners. This tissue-specific response to a given insult with oxidative stress has previously been recognized [44,49]. As in the present study, Jun et al. [49] found that, in comparison to other tissues, liver is the organ with the highest susceptibility to oxidative stress in response to IH. As the liver is the central organ of the metabolism, our findings should increase the understanding of the great number of metabolic alterations in OSAS patients. Going a step further, our study shows that oxidative stress of the liver is associated with an activation of NF-κB and CRP production in hepatic cells as well as with the initiation of nonalcoholic fatty liver disease and increased plasma triglycerides and cholesterol. Although a search for the nature of this association was not undertaken in this study, it might be suggested, as is the case in other systems, that oxidative stress is causally linked to NF-κB activation and subsequent inflammatory and metabolic alterations [44,50,51]. Thus, the present findings, showing that IH of even moderate intensity causes oxidative stress, solve a long-lasting and currently ongoing controversy (see [13] vs [14]): oxidative stress must be considered a primary mechanism in the pathogenesis of the comorbidities present in OSAS, reflected in our study by the augmented fat content in liver and increased plasma lipid levels. Despite this conclusion, we do not intend to neglect the very significant role of the CB sensitization to hypoxia in the genesis of an augmented sympathetic activity and its contribution to cardiovascular and metabolic pathologies encountered in OSAS patients and IH animals [13,17,18].

Data presented in Table 1B indicate that the assessment of the severity of the IH encountered in experimental models, and certainly in OSAS patients, requires knowledge of the SaO_2-related parameters such as $ASaO_2$, $LSaO_2$, and $T<90\%$. The AHI and ODI would not suffice as criteria of OSAS severity. Additionally, Table 1B makes it clear that IH models do not mimic all features of OSA. Thus, although there is an increase in arterial PCO_2 in the clinical situation accompanying each episode of hypoxia (see the introduction), in the laboratory model, the hypoxic episode is accompanied by a decrease in arterial PCO_2 (Table1B). Yet, as stated in the introduction, it is accepted that hypoxia would represent the element of inadequate respiration in OSA that most likely leads to systemic pathology. In fact, Fletcher et al. [3], soon after they developed the current IH model, demonstrated that the relevant hypertension-generating factor was the episodic hypoxia, which in itself causes hypocapnia, and that the addition of CO_2 to make the episodic hypoxia eucapnic or moderately hypercapnic (as occurs in OSAS patients) does not augment the hypertension. There are no data on the effects of PCO_2/pH oscillations on redox status, but, to our understanding, there are no reasons to suspect major modulations of the effects produced by the hypoxic episodes.

The data of Table 2 and Fig. 1 evidence the normality of glutathione levels and redox potential in the tissues of both IH groups. These findings, which agree with those of other authors (e.g., [49,52]), were to some extent expected. GSH/GSSG content in cells is in the millimolar range (or about 1000 times higher than the LPO levels), evidencing the great capacity of cells to eliminate hydrogen peroxide and the need for an exaggerated ROS production to cause a decrease in GSH levels or E_{GSH}. In turn, the maintenance of the E_{GSH} is a prerequisite for cell survival preventing the starting of apoptotic processes [38]. At the same time, the findings on glutathione show that the use of a single marker to assess the redox status can lead to erroneous conclusions, as other markers unequivocally demonstrate that, in the same animals and tissues, there is indeed oxidative damage (see below).

The increase in LPO levels is restricted to liver tissue. A liver-specific upregulated expression and activation of NADPH oxidase by IH has previously been demonstrated, with a link between NADPH oxidase-derived ROS and lipid peroxidation also being suggested [49]. However, our data from Fig. 3 would indicate that mitochondria-derived ROS could also contribute to increased LPO levels in liver. In fact several authors have evidenced bidirectional cross talk between mitochondrial and NADPH oxidase-derived ROS in several cell models and in response to various stimuli. For example, in endothelial cells, angiotensin II produces an initial augmentation of ROS production due to the activation of NADPH oxidase, which in turn triggers a secondary activation of ROS production in mitochondria (for references see [53]). In pulmonary artery smooth muscle cells it has been observed that hypoxia causes a prompt production of ROS in mitochondria with mitochondrial-derived ROS leading to the activation of NADPH oxidase via a protein kinase C-mediated pathway [53,54]. Whatever the sequence of events (not explored in this study), the decrease in the aconitase/fumarase activity ratio seen with the more intense IH (Fig. 3), which evidences an increase in superoxide anion production in mitochondria, is fully consistent with those proposals.

The mechanisms leading to increased ROS production in hypoxia are complex and not unequivocally solved. Schumacker and coworkers have proposed in an ample series of articles (see [55]) that hypoxia per se directly causes an increase in ROS production at the level of mitochondrial complex III. Their proposal is that fully reduced ubiquinol diffuses to complex III, where it binds to the inner membrane (the Qo site). The transfer of electrons from ubiquinol follows a precise order, with the first electron being transferred to the Rieske iron–sulfur protein, resulting in the formation of the ubisemiquinone radical. Ubisemiquinone normally transfers its remaining electron to the cytochromes *b* in complex III; however, this free radical can alternatively transfer its electron to O_2, yielding $O_2^{\bullet -}$. In either case, the resulting oxidized molecule (ubiquinone) reenters the so-called quinone pool ready to accept a new pair of electrons from complex I and/or II to become ubiquinol and restart the cycle [55,56]. However, how this mechanism of electron transfer to molecular O_2 could paradoxically increase during hypoxia is not known [55,57]. In fact, the formation of $O_2^{\bullet -}$ by the transfer of a single electron to molecular O_2 is directly dependent on the oxygen concentration [56], and obviously, in hypoxia, the O_2 concentration decreases. Therefore, some additional factor(s) must enter into play to explain the increased rates of ROS production in hypoxia [56,58]. According to Taylor and Moncada [59] nitric oxide could be the factor. Thus, whereas in normoxia reduced cytochrome oxidase binds nitric oxide and oxidizes it to nitrite, in hypoxia, as the cytochrome oxidase is becoming reduced, nitric oxide competes with O_2 in binding to the cytochrome oxidase and inhibits the enzyme. This inhibition results in nitric oxide accumulation, back reduction of the entire respiratory chain, facilitation of the leaking of single electrons to upstream complexes of the respiratory chain, and the formation of $O_2^{\bullet -}$ (see also [56]). This interpretation would explain the observed decrease in aconitase activity, because $O_2^{\bullet -}$ is the main factor responsible for the disruption of the $[4Fe–4S]^{2+}$ cluster present in the enzyme and the abolition of its functional activity [40].

Similarly, the interpretation given in the previous paragraph would contribute to the observations presented in Fig. 4 in which a marked decrease in the activity of liver Mn-SOD is evident. An increase in $O_2^{\bullet -}$ and nitric oxide would generate peroxynitrite, which in turn would nitrate the tyrosine 34 residue of the enzyme, leading to its inactivation [60]. In a similar manner, peroxynitrite can nitrate a tryptophan residue present in Cu,Zn-SOD, leading to its inactivation [60]. However, the regulation of SODs seems to be more complex. It is commonly observed that the ROS-dependent activation of NF-κB (see below) leads to an increase in SOD expression, it being accepted that these mechanistically linked events are important to maintain intracellular oxidant–antioxidant homeostasis (see [61]). But these sequences of events are not seen in all cell types or in response to all stimuli (see [62]). We found that IH diminishes Mn-SOD expression by about 25 and 35% (10 and 5% O_2, respectively), but diminishes activity by around 70%, implying, on one hand, that IH downregulates the expression of the enzyme and, on the other, that as a whole, the translated Mn-SOD molecules have a lower level of intrinsic activity, probably as a result of the oxidative damage mentioned above. Consistent with the decreased Mn-SOD expression found in our study, Nanduri et al. [63] also observed that IH causes a decrease in MnSOD protein expression in vivo, in the same model used in our experiments. Additionally, these authors [63], using another model of IH in cultured cells, were able to state that the decreased Mn-SOD transcription was due to a decrease in the levels of HIF-2α, which in turn resulted from a calpain-dependent degradation of this transcription factor. To sum up, the overall control of SOD activity in IH, and in particular the control of Mn-SOD, is multifactorial, with the final outcome that there is a marked diminution of the dismutating capacity of liver and brain cells of animals subjected to intense IH. In contrast to mitochondrial enzyme, IH does not affect Cu,Zn-SOD expression and therefore the diminution of Cu,Zn-SOD activity should be attributed to direct ROS damage of the enzyme molecule [60]. Regarding catalase, our data unequivocally indicate that intense IH causes a diminution of the expression of catalase without affecting its specific activity, as the ratio catalase activity/catalase protein was nearly identical to that seen in control animals. Because Haque et al. [64] have recently shown in a human retinal pigment epithelial cell line that oxidative stress causes a microRNA-mediated posttranscriptional inhibition of the catalase expression, we would hypothesize that the decrease in catalase enzyme expression seen in our

experiments might be the result of a comparable posttranscriptional mechanism.

On the other hand, the mechanisms of ROS-dependent activation of NF-κB are well established in many cell systems [44,50,51]. Members of the NF-κB family are complexed in the cell cytoplasm with the inhibitory κB subunit, which upon phosphorylation by the redox-sensitive inhibitory κB kinase, is dissociated from the NF-κB complex, ubiquitinated, and degraded in a proteasome-dependent manner. Freed NF-κB members (p65/p50) form heterodimers that translocate to the nucleus and bind to the promoters of the regulated genes, among other inflammatory cytokines; after DNA binding, NF-κB is transported back to the cytosol and recycled [51,65]. This chain of events would lead to the proinflammatory status encountered in experimental IH as well as in OSAS patients.

The decrease in the activity of aconitase can satisfactorily explain the observed accumulation of fat in the liver. First, our data evidence a clear parallelism between both alterations; only the more intense IH decreased aconitase activity. Second, Lanaspa et al. [66], working with a human hepatocyte cell line, demonstrated that a decrease in aconitase activity, due to oxidative damage, produces an accumulation of citrate in the mitochondria because the citrate produced by citrate synthase cannot be isomerized by aconitase. As a consequence, citrate would be exported to the cell cytoplasm, causing a stimulation of ATP citrate lyase and fatty acid synthase leading to de novo lipogenesis and hepatic fat accumulation (see also [41]). Finally, augmented liver lipogenesis would contribute to explaining the observed hyperlipidemia (Fig. 8 and [41,66]), although a peripheral diminution of the clearance of triglyceride-rich lipoproteins would seem to be the prime factor causing the elevation of triglycerides and cholesterol observed in IH [67].

We do not wish to conclude this discussion without explicitly pointing out what could be considered a limitation of this study. The fact that our work is not mechanistically oriented implies that some of the causal links proposed throughout the discussion are based on our best understanding of the current literature, but are not experimentally proven. It must be added, however, that this possible limitation has been imposed by the nature of the specific aim of our study. The fundamental and most urgent aim, as it emerges from current controversy in the literature (see the introduction), has been to define whether IH, the primary element causing OSA-associated comorbidities, causes oxidative stress. qIn accomplishing this specific aim, we have had to use an ample spread of techniques, apply them to three key body tissues, and use two intensities of IH. This wide experimental approach has resulted in the clear definition of the tissue specificity of oxidative damage produced by IH, and therefore this study could well direct future studies in searching for specific mechanisms in specific organs or for the efficacy of pharmacological strategies (e.g., antioxidant therapies).

In conclusion, our study demonstrates that IH of even moderate intensity produced an oxidative status that is organ specific, liver tissue being the most sensitive tissue studied. This oxidative status reflected by an augmentation of LPO and a decrease in the aconitase/fumarase activity ratios, as well as modifications in the activities of ROS-detoxifying enzymes, leads in liver to an increased activation of NF-κB and secretion of CRP and a concomitant increase in plasma CRP levels. The decrease in aconitase activity most probably generates an increased rate of fatty acid synthesis, thereby explaining the observed augmentation in liver lipid content and hyperlipidemia.

Authors' contributions

Constancio Gonzalez, Ana Obeso, Ramón Farre, Teresa Agapito, and Sara Yubero participated in the research design. Miguel Quintero, Carmen Gonzalez-Martín, Mª Victoria Vega-Agapito, Ana Obeso, Teresa Agapito, and Sara Yubero conducted the experiments. Miguel Quintero, Carmen Gonzalez-Martín, Mª Victoria Vega-Agapito, Ana Obeso, Constancio Gonzalez, Teresa Agapito, and Sara Yubero performed data analysis. Constancio Gonzalez, Sara Yubero, and Ramón Farre wrote or contributed to the writing of the manuscript. All authors proofread the manuscript and contributed to its improvement. Constancio Gonzalez and Ramon Farré obtained financial support.

Acknowledgments

We thank Mª de los Llanos Bravo, Elena Olea, and Ana Gordillo for their technical assistance. Thanks are due to Alan Hynds for his linguistic assistance. This work was supported by the Spanish Ministry of Science and Innovation (Grants BFU2007-61848 to Constancio Gonzalez and SAF2011-22576 to Ramon Farre); the Spanish Ministry of Economy and Competitiveness (Grant BFU2012-37459 to Constancio Gonzalez), and the Spanish Ministry of Health–Institute Carlos III (Grant CIBER CB06/06/0050 to Constancio Gonzalez and Ramón Farre). Part of this work was included in the Ph.D. thesis of Carmen Gonzalez-Martin (University of Valladolid, Spain).

Appendix A. Supplementary material

Supplementary data associated with this article can be found in the online version at http://dx.doi.org/10.1016/j.freeradbiomed.2013.08.180.

References

[1] Ryan, CM; Bradley, TD. Pathogenesis of obstructive sleep apnea. *J. Appl. Physiol.* **99:**2440–2450; 2005.
[2] Tsai, YJ; Ramar, K; Liang, YJ; Chiu, PH; Powell, N; Chi, CY; Lung, TC; Wen-Yang Lin, W; Tseng, PJ; Wu, MY; Chien, KC; Weaver, EM; Lee, FP; Lin, CM; Chen, KC; Chiang, RP. Peripheral neuropathology of the upper airway in obstructive sleep apnea syndrome. *Sleep Med. Rev* **17:**161–168; 2013.
[3] Fletcher, EC; Bao, G; Miller 3rd CC Effect of recurrent episodic hypocapnic, eucapnic, and hypercapnic hypoxia on systemic blood pressure. *J. Appl. Physiol* **78:**1516–1521; 1995.
[4] Chaudhary, B; Dasti, S; Park, Y; Brown, T; Davis, H; Akhtar, B. Hour-to-hour variability of oxygen saturation in sleep apnea. *Chest* **113:**719–722; 1998.
[5] Adamson, PB. Beyond the apnea–hypopnea index—prognostic value of other elements of polysomnography to describe sleep-disordered breathing in heart failure. *US Cardiol* **6(2):**68–71; 2009.
[6] Gonzalez, C; Almaraz, L; Obeso, A; Rigual, R. Carotid body chemoreceptors: from natural stimuli to sensory discharges. *Physiol. Rev.* **74:**829–898; 1994.
[7] Terán-Santos, J; Jiménez-Gómez, A; Cordero-Guevara, J. The association between sleep apnea and the risk of traffic accidents. *Cooperative Group Burgos-Santander. N. Engl. J. Med* **340:**847–851; 1999.
[8] Marrone, O; Bonsignore, MR. Pulmonary haemodynamics in obstructive sleep apnoea. *Sleep Med. Rev.* **6:**175–193; 2002.
[9] Almendros, I; Montserrat, JM; Torres, M; Gonzalez, C; Farré, Navajas D Changes in oxygen partial pressure of brain tissue in an animal model of obstructive apnea. *Respir. Res* **15:**11–13; 2010.
[10] Sateia, MJ. Neuropsychological impairment and quality of life in obstructive sleep apnea. *Clin. Chest Med* **24:**249–259; 2003.
[11] Martínez-García, MA; Durán-Cantolla, J Montserrat JM. Sleep apnea–hypopnea syndrome in the elderly. *Arch. Bronconeumol* **46:**479–488; 2010.
[12] Thomas, JJ; Ren, J. Obstructive sleep apnea and cardiovascular complications: perception versus knowledge. *Clin. Exp. Pharmacol. Physiol.* **39:**995–1003; 2012.
[13] Kohler, M; Stradling, JR. CrossTalk proposal: most of the cardiovascular consequences of OSA are due to increased sympathetic activity. *J. Physiol* **590:**2813–2815; 2012.
[14] Lavie, L; Lavie, P. CrossTalk opposing view: most cardiovascular diseases in sleep apnoea are not caused by sympathetic activation. *J. Physiol* **590:** 2817–2819; 2012.
[15] Mills, PJ; Kennedy, BP; Loredo, JS; Dimsdale, JE; Ziegler, MG. Effects of nasal continuous positive airway pressure and oxygen supplementation on norepinephrine kinetics and cardiovascular responses in obstructive sleep apnea. *J. Appl. Physiol* **100:**343–348; 2006.
[16] Kohler, M; Stoewhas, AC; Ayers, L; Senn, O; Bloch, KE; Russi, EW; Stradling, JR. Effects of continuous positive airway pressure therapy withdrawal in patients

with obstructive sleep apnea: a randomized controlled trial. *Am. J. Respir. Crit. Care Med* **184:**1192–1199; 2011.
[17] Lesske, J; Fletcher, EC; Bao, G; Unger, T. Hypertension caused by chronic intermittent hypoxia—influence of chemoreceptors and sympathetic nervous system. *J. Hypertens* **15:**1593–1603; 1997.
[18] Prabhakar, NR; Peng, YJ; Jacono, FJ; Kumar, GK; Dick, TE. Cardiovascular alterations by chronic intermittent hypoxia: importance of carotid body chemoreflexes. *Clin. Exp. Pharmacol. Physiol.* **32:**447–449; 2005.
[19] Lavie, L. Obstructive sleep apnoea syndrome—an oxidative stress disorder. *Sleep Med. Rev* **7:**35–51; 2003.
[20] Lavie, L; Lavie, P. Molecular mechanisms of cardiovascular disease in OSAHS: the oxidative stress link. *Eur. Respir. J.* **33:**1467–1484; 2009.
[21] Oztürk, L; Mansour, B; Yüksel, M; Yalçin, AS; Celikoğlu, F; Gökhan, N. Lipid peroxidation and osmotic fragility of red blood cells in sleep-apnea patients. *Clin. Chim. Acta* **332:**83–88; 2003.
[22] Svatikova, A; Wolk, R; Lerman, LO; Juncos, LA; Greene, EL; McConnell, JP; Somers, VK. Oxidative stress in obstructive sleep apnoea. *Eur. Heart J.* **26:**2435–2439; 2005.
[23] Barceló, A; Barbé, F; de la Peña, M; Vila, M; Pérez, G; Piérola, J; Durán, J; Agustí, AG. Antioxidant status in patients with sleep apnoea and impact of continuous positive airway pressure treatment. *Eur. Respir. J.* **27:**756–760; 2006.
[24] Kohler, M; Ayers, L; Pepperell, JC; Packwood, KL; Ferry, B; Crosthwaite, N; Craig, S; Siccoli, MM; Davies, RJ; Stradling, JR. Effects of continuous positive airway pressure on systemic inflammation in patients with moderate to severe obstructive sleep apnoea: a randomised controlled trial. *Thorax* **64:**67–73; 2009.
[25] Gonzalez, C; Sanz-Alfayate, G; Obeso, A; Agapito, MT. Role of glutathione redox state in oxygen sensing by carotid body chemoreceptor cells. *Methods Enzymol* **381:**40–71; 2004.
[26] Siems, W; Grune, T. Lipid peroxidation measurements: methodological approaches and clinical importance. In: Grune, T., editor. *Free Radicals and Diseases: Gene Expression, Cellular Metabolism and Pathophysiology*. Amsterdam: IOS Press; 2005. p. 11–22.
[27] Calvo, JR; Reiter, RJ; García, JJ; Ortiz, GG; Tan, DX; Karbownik, M. Characterization of the protective effects of melatonin and related indoles against alpha-naphthylisothiocyanate-induced liver injury in rats. *J. Cell. Biochem* **80:**461–470; 2001.
[28] Couplan, E; del Mar Gonzalez-Barroso, M; Alves-Guerra, MC; Ricquier, D; Goubern, M; Bouillaud, F. No evidence for a basal, retinoic, or superoxide-induced uncoupling activity of the uncoupling protein 2 present in spleen or lung mitochondria. *J. Biol. Chem* **277:**26268–26275; 2002.
[29] Pecqueur, C; Alves-Guerra, MC; Gelly, C; Levi-Meyrueis, C; Couplan, E; Collins, S; Ricquier, D; Bouillaud, F; Miroux, B. Uncoupling protein 2, in vivo distribution, induction upon oxidative stress, and evidence for translational regulation. *J. Biol. Chem* **276:**8705–8712; 2001.
[30] Hausladen, A; Fridovich, I. Measuring nitric oxide and superoxide: rate constants for aconitase reactivity. *Methods Enzymol* **269:**37–41; 1996.
[31] Racker, E. Spectrophotometric measurements of the enzymatic formation of fumaric and cis-aconitic acids. *Biochim. Biophys. Acta* **4:**211–214; 1950.
[32] Paglia, DE; Valentine, WN. Studies on the quantitative and qualitative characterization of erythrocyte glutathione peroxidase. *J. Lab. Clin. Med* **70:**158–169; 1967.
[33] Aebi, H. Catalase in vitro. *Methods Enzymol.* **105:**121–126; 1984.
[34] Caceres, AI; Obeso, A; Gonzalez, C; Rocher, A. Molecular identification and functional role of voltage-gated sodium channels in rat carotid body chemoreceptor cells: regulation of expression by chronic hypoxia in vivo. *J. Neurochem* **102:**231–245; 2007.
[35] Folch, J; Lees, M; Sloane Stanley, GH. A simple method for the isolation and purification of total lipids from animal tissues. *J. Biol. Chem* **226:**497–509; 1957.
[36] Dikmenoğlu, N; Ciftçi, B; Ileri, E; Güven, SF; Seringeç, N; Aksoy, Y; Ercil, D. Erythrocyte deformability, plasma viscosity and oxidative status in patients with severe obstructive sleep apnea syndrome. *Sleep Med* **7:**255–261; 2006.
[37] Peled, N; Kassirer, M; Kramer, MR; Rogowski, O; Shlomi, D; Fox, B; Berliner, AS; Shitrit, D. Increased erythrocyte adhesiveness and aggregation in obstructive sleep apnea syndrome. *Thromb. Res* **121:**631–636; 2008.
[38] Schafer, FQ; Buettner, GR. Redox environment of the cell as viewed through the redox state of the glutathione disulfide/glutathione couple. *Free Radic. Biol. Med* **30:**1191–1212; 2001.
[39] Halliwell, B *Gutteridge JMC. Free Radicals in Biology and Medicine*. 3rd edition. Oxford: Oxford Univ. Press; 1999.
[40] Bulteau, AL; Ikeda-Saito, M; Szweda, LI. Redox-dependent modulation of aconitase activity in intact mitochondria. *Biochemistry* **42:**14846–14855; 2003.
[41] Yarian, CS; Toroser, D; Sohal, RS. Aconitase is the main functional target of aging in the citric acid cycle of kidney mitochondria from mice. *Mech. Ageing Dev* **127:**79–84; 2006.
[42] Kinnula, VL; Crapo, JD. Superoxide dismutases in the lung and human lung diseases. *Am. J. Respir. Crit. Care Med.* **167:**1600–1619; 2003.
[43] Lijnen, PJ; van Pelt, JF; Fagard, RH. Stimulation of reactive oxygen species and collagen synthesis by angiotensin II in cardiac fibroblasts. *Cardiovasc. Ther* **30:** e1–8; 2012.
[44] Criswell, T; Leskov, K; Miyamoto, S; Luo, G; Boothman, DA. Transcription factors activated in mammalian cells after clinically relevant doses of ionizing radiation. *Oncogene* **22:**5813–5827; 2003.
[45] Zhang, Z; Yang, Y; Hill, MA; Wu, J. Does C-reactive protein contribute to atherothrombosis via oxidant-mediated release of pro-thrombotic factors and activation of platelets? *Front. Physiol* **3:**433; 2012.
[46] Videla, LA; Rodrigo, R; Araya, J; Poniachik, J. Insulin resistance and oxidative stress interdependency in non-alcoholic fatty liver disease. *Trends Mol. Med* **12:**555–558; 2006.
[47] de Oliveira, CP; Simplicio, FI; de Lima, VM; Yuahasi, K; Lopasso, FP; Alves, VA; Abdalla, DS; Carrilho, FJ; Laurindo, FR; de Oliveira, MG. Oral administration of S-nitroso-N-acetylcysteine prevents the onset of non alcoholic fatty liver disease in rats. *World J. Gastroenterol* **12:**1905–1911; 2006.
[48] Zhang, D; Xie, L; Jia, G; Cai, S; Ji, B; Liu, Y; Wu, W; Zhou, F; Wang, A; Chu, L; Wei, Y; Liu, J; Gao, F. Comparative study on antioxidant capacity of flavonoids and their inhibitory effects on oleic acid-induced hepatic steatosis in vitro. *Eur. J. Med. Chem* **46:**4548–4558; 2011.
[49] Jun, J; Savransky, V; Nanayakkara, A; Bevans, S; Li, J; Smith, PL; Polotsky, VY. Intermittent hypoxia has organ-specific effects on oxidative stress. *Am. J. Physiol. Regul. Integr. Comp. Physiol* **295:**R1274–1281; 2008.
[50] Bowie, A; O'Neill, LA. Oxidative stress and nuclear factor-kappa B activation: a reassessment of the evidence in the light of recent discoveries. *Biochem. Pharmacol* **59:**13–23; 2000.
[51] Korkmaz, A; Rosales-Corral, S; Reiter, RJ. Gene regulation by melatonin linked to epigenetic phenomena. *Gene* **503:**1–11; 2012.
[52] Savransky, V; Reinke, C; Jun, J; Bevans-Fonti, S; Nanayakkara, A; Li, J. Chronic intermittent hypoxia and acetaminophen induce synergistic liver injury in mice. *Exp. Physiol* **94:**228–239; 2009.
[53] Daiber, A. Redox signaling (cross-talk) from and to mitochondria involves mitochondrial pores and reactive oxygen species. *Biochim. Biophys. Acta* **1797:**897–906; 2010.
[54] Frazziano, G; Moreno, L; Moral-Sanz, J; Menendez, C; Escolano, L; Gonzalez, C; Villamor, E; Alvarez-Sala, JL; Cogolludo, AL; Perez-Vizcaino, F. Neutral sphingomyelinase, NADPH oxidase and reactive oxygen species: role in acute hypoxic pulmonary vasoconstriction. *J. Cell Physiol* **226:**2633–2640; 2011.
[55] Schumacker, PT. Lung cell hypoxia: role of mitochondrial reactive oxygen species signaling in triggering responses. *Proc. Am. Thorac. Soc* **8:**477–484; 2011.
[56] Turrens, JF. Mitochondrial formation of reactive oxygen species. *J. Physiol.* **552:**335–344; 2003.
[57] Waypa, GB; Schumacker, PT. Oxygen sensing in hypoxic pulmonary vasoconstriction: using new tools to answer an age-old question. *Exp. Physiol* **93:**133–138; 2008.
[58] Jezek, P; Hlavatá, L. Mitochondria in homeostasis of reactive oxygen species in cell, tissues, and organism. *Int. J. Biochem. Cell. Biol.* **37:**2478–2503; 2005.
[59] Taylor, CT; Moncada, S. Nitric oxide, cytochrome C oxidase, and the cellular response to hypoxia. *Arterioscler. Thromb. Vasc. Biol.* **30:**643–647; 2010.
[60] Yamakura, F; Kawasaki, H. Post-translational modifications of superoxide dismutase. *Biochim. Biophys. Acta* **318-325:**2010; 1804.
[61] Ji, LL. Modulation of skeletal muscle antioxidant defense by exercise: role of redox signaling. *Free Radic. Biol. Med* **44:**142–152; 2008.
[62] Lijnen, PJ; van Pelt, JF; Fagard, RH. Stimulation of reactive oxygen species and collagen synthesis by angiotensin II in cardiac fibroblasts. *Cardiovasc. Ther.* **30:** e1–8; 2012.
[63] Nanduri, J; Wang, N; Yuan, G; Khan, SA; Souvannakitti, D; Peng, YJ; Kumar, GK; Garcia, JA; Prabhakar, NR. Intermittent hypoxia degrades HIF-2alpha via calpains resulting in oxidative stress: implications for recurrent apnea-induced morbidities. *Proc. Natl. Acad. Sci. USA* **106:**1199–1204; 2009.
[64] Haque, R; Chun, E; Howell, JC; Sengupta, T; Chen, D; Kim, H. MicroRNA-30b-mediated regulation of catalase expression in human ARPE-19 cells. *PLoS One* **7:**e42542; 2012.
[65] Kim, H. Inhibitory mechanism of lycopene on cytokine expression in experimental pancreatitis. *Ann. N. Y. Acad. Sci* **1229:**99–102; 2011.
[66] Lanaspa, MA; Sanchez-Lozada, LG; Choi, YJ; Cicerchi, C; Kanbay, M; Roncal-Jimenez, CA; Ishimoto, T; Li, N; Marek, G; Duranay, M; Schreiner, G; Rodriguez-Iturbe, B; Nakagawa, T; Kang, DH; Sautin, YY; Johnson, RJ. Uric acid induces hepatic steatosis by generation of mitochondrial oxidative stress: potential role in fructose-dependent and -independent fatty liver. *J. Biol. Chem* **287:**40732–40744; 2012.
[67] Drager, LF; Li, J; Shin, MK; Reinke, C; Aggarwal, NR; Jun, JC; Bevans-Fonti, S; Sztalryd, C; O'Byrne, SM; Kroupa, O; Olivecrona, G; Blaner, WS; Polotsky, VY. Intermittent hypoxia inhibits clearance of triglyceride-rich lipoproteins and inactivates adipose lipoprotein lipase in a mouse model of sleep apnoea. *Eur. Heart J.* **33:**783–790; 2012.